be measured by tracking any of the freely falling devices. An alternative would be to launch a sounding rocket simultaneously with the launch vehicle. Since it will rise much faster than the launch vehicle, an alkali vapor ejected from it would be a good measure of the wind actually existing at the time of the launch vehicle ascent.

References

[1] Cato, G. A., "Ultra-high altitude measurement systems for pressure, density, temperature and wind," NASA Contract NAS8-5226, Electro-Optical Systems, Inc., Rept. 3780-Final (November 1963).

[2] *U. S. Standard Atmosphere, 1962* (U. S. Government Printing Office, Washington, D. C., 1962).

[3] Ragsdale, G. C. and Wasko, P. E., "Wind flow in the 80–400 km altitude region of the atmosphere," NASA TN D-1573 (March 1963).

[4] LaGow, H. E., Horowitz, R., and Ainsworth, J., "Arctic atmosphere structure to 250 km," Planetary Space Sci. 2, 356–361 (October 1959).

[5] Ainsworth, J. E., Fox, D. F., and LaGow, H. E., "Measurement of upper atmosphere structure by means of the pitot static tube," NASA TN D-670 (February 1961).

[6] Belcher, J. T. and Gilbert, B. S., "Qualification of F-16 Q-Ball and total temperature measurements on board vehicle SA-4," NASA George C. Marshall Space Flight Center MTP-AERO-63-57 (July 1963); confidential.

[7] Glass, D. R., "Methods for measuring ambient air temperatures from high speed aircraft," Univ. of Michigan Engineering Research Institute, Wright Air Development Center TR 57-705, Armed Services Technical Information Agency AD 142169 (December 1957).

[8] Barnes, T. G. and McDonald, C., "Determination of atmospheric parameters by acoustic means," Schellenger Research Lab., Texas Western College Progr. Rept. I, Armed Services Technical Information Agency AD 297431 (July 1962).

[9] Kalinovskiy, A. B. and Pinus, N. Z., "Soviet aerological measurement," U. S. Dept. of Commerce JPRS Doc. 16691, Armed Services Technical Information Agency AD 292217 (December 17, 1962).

[10] Astheimer, R. W., "An infrared radiation air thermometer," Barnes Engineering Co. Tech. Paper, Stamford, Conn. (October 1962).

[11] Swalley, F. E., "Measurement of flow angularity at supersonic and hypersonic speeds with the use of a conical probe," NASA L-1216 (1961).

[12] Baur, J. P. and Belcher, J. T., "F-16 Q-ball data reduction technique and angle of attack evaluation on Saturn SA-4," NASA George C. Marshall Space Flight Center MTP-AERO-63-48 (June 1963).

[13] Nagy, A. F., et al., "Measurements of atmospheric pressure, temperature and density at very high altitudes," Univ. of Michigan College of Engineering, ORA Projects 02804, 04004, and 04141 (August 1961).

MAY-JUNE 1965 J. SPACECRAFT VOL. 2, NO. 3

Feasibility of Large Launch Vehicle Recovery

S. A. MILLIKEN*
Hughes Aircraft Company, El Segundo, Calif.

Recovery of stages of large two-stage launch vehicles is examined for two design approaches: 1) the basic expandable stage is adapted for recovery by adding recovery equipment and strengthening the basic vehicle for repeated launches and recoveries, or 2) the basic vehicle is designed for recovery in an optimum manner by shaping the vehicle to achieve aerodynamic stability for the re-entry and terminal descent phase. Aerodynamic loads are calculated to be ≤ 15 g's for either stage. Thermal protection for the first stage is required for small thin-walled structures only; large structures absorb the aerodynamic heating without exceeding allowable temperatures. All exposed second-stage structure requires thermal protection. Terminal deceleration is best accomplished by a combination of parachutes and rocket decelerators. Water alighting loads are estimated to be 10 g's if the rocket decelerators bring the recovered stage to a hovering condition over the water. An economic estimate indicates that use of first-stage recovery in a program consisting of 100 launches could reduce direct operating cost by 33% and over-all program cost by 20%.

Nomenclature

a = acceleration, ft/sec^2
A, B = const (in equations for rocket motor weights)
C_D = vehicle drag coefficient
F = rocket decelerator thrust, lb
g = earth's gravitational acceleration
h_s = enthalpy of air stream at stagnation point, Btu/lb
h_w = enthalpy of air at wall surface, Btu/lb
h_{300} = enthalpy of air at 300°C, Btu/lb
I_s = specific impulse, sec
N = deceleration, $N \equiv (F/W) - 1$, g
K = const (in equations for water alighting loads)
p = pressure, psf
$\dot{q}_c$ = stagnation-point convective heat-transfer rate, Btu/ft^2-sec
R_n = nose radius of curvature, ft
t = time from retrorocket ignition, sec
V = instantaneous velocity, fps
V_0 = initial velocity, fps
W = vehicle weight, lb
W_r = retrorocket weight, lb

Presented as Preprint 63-247 at the AIAA Summer Meeting, Los Angeles, Calif., June 17–20, 1963; revision received January 20, 1965. This investigation was part of the NOVA Study, Phase I, conducted under the direction of the Marshall Space Flight Center, NASA, at General Dynamics/Astronautics. The writer wishes to acknowledge consultation and technical assistance from J. P. Wamser, R. C. Ferguson, C. C. Love, and W. Kanpton of General Dynamics/Astronautics; R. T. Hopkins of Convair; and personnel of the Cook Technological Center, Raven Industries, the Goodyear Aircraft Company, Northrop Ventura, and the Irvine Air Chute Company.

* Project Engineer, Space Systems Division; formerly Preliminary Design Engineer, General Dynamics/Astronautics, San Diego, Calif. Member AIAA.

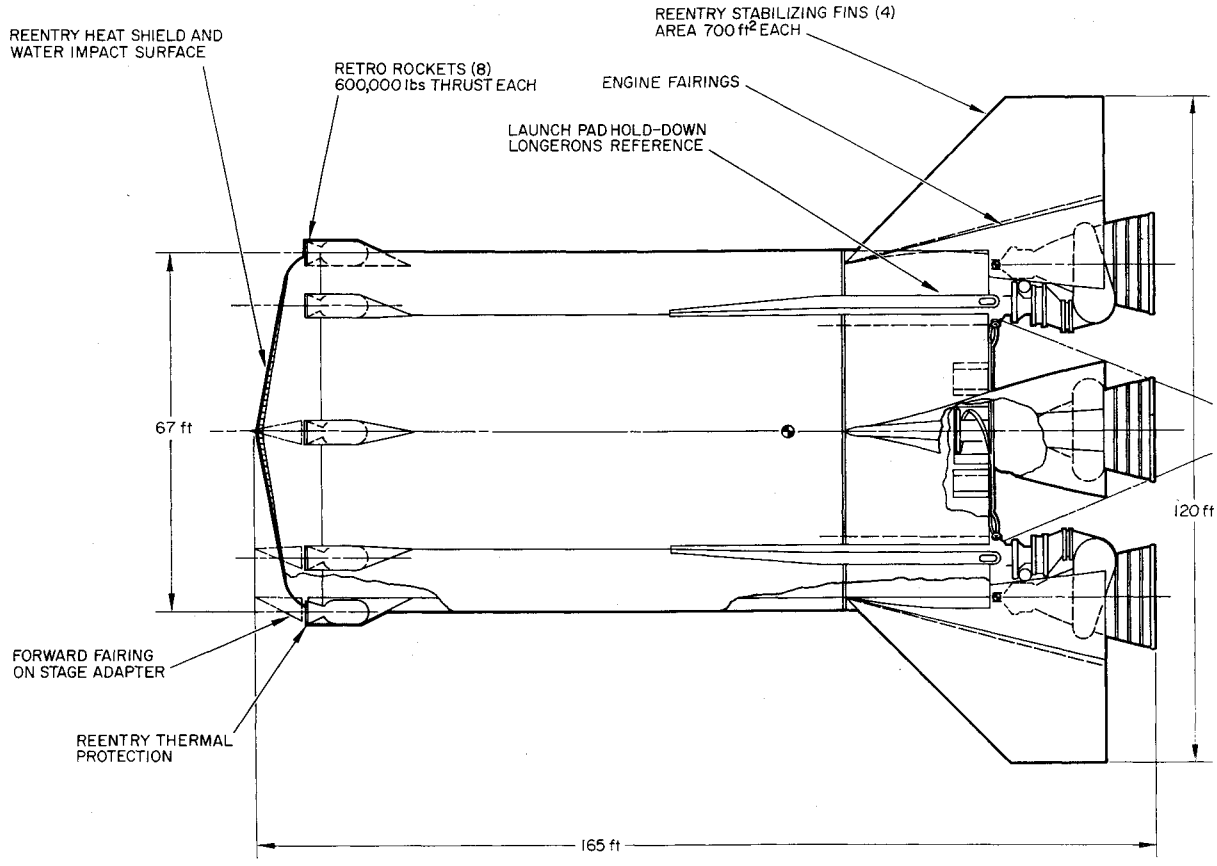

Fig. 1 Recoverable launch vehicle, configuration I.

W_p = propellant weight, lb
W_{pay} = payload weight, lb
x = vehicle longitudinal station, in.
y = vehicle lateral stations, in.
ρ = water density, atmosphere density, lb/ft³
ρ_0 = sea-level atmosphere density, lb/ft³
ρ_∞ = freestream atmosphere density, lb/ft³

Introduction

A PRACTICAL, lightweight recovery system for large launch vehicle stages would reduce program costs. Secondary benefits would accrue from the possibility of improving the basic vehicle design as a result of the inspection of the systems and components which have undergone actual flight experience. The present paper examines the technical feasibility of recovery of large rocket booster stages. Since the weight of each empty stage exceeds the gross weight of the largest aircraft, reappraisal of recovery techniques is required to determine feasibility. The results obtained in selected critical design areas are presented in parametric form to facilitate preliminary design studies of recoverable launch vehicles.

The study is based on a two-stage launch vehicle for missions requiring injection into low-altitude circular earth orbit. Staging velocity for an expendable vehicle is selected to minimize the cost of injecting a given payload into orbit, and stage recovery studies are performed about this optimum cost point. First-stage burnout occurs at approximately 11,000 fps for liquid-propellant launch vehicles using liquid oxygen and hydrocarbon propellants for the first stage and with liquid oxygen and liquid hydrogen propellants for the second stage. The first stage follows a ballistic path following separation with a range of approximately 700 naut miles to the recovery area. Second-stage recovery may be initiated after one or more orbits. Second-stage recovery operations could, therefore, be carried out near the launch site.

Design Approaches

During atmospheric entry, the recoverable body should be oriented in a preferred direction to receive the deceleration loads; this requires both static and dynamic stability. Aerodynamic stability may be obtained through the use of inflated structures, the addition of fins, or by proper shaping of the body. Initial orientation to the preferred direction would be desirable, but it is not expected to be required for all approaches. If aerodynamic stability is to effect the reorientation during the initial period of re-entry, the recoverable body should exhibit only one statically stable orientation. This criterion is generally met with cone-cylinder-fin or cone-cylinder-flare configurations. Body configurations that approach ellipsoids of revolution, however, exhibit two stable points that are diametrically opposed. This latter configuration could either be equipped with initial orientation controls or a high-drag device could be trailed to establish the preferred orientation.

Two general design approaches are considered. The first consists of adapting the basic expendable vehicle configuration to recovery through the addition of a heat shield, stabilizing fins, and a terminal deceleration system. A recoverable first-stage configuration with static aerodynamic stability is shown in Fig. 1. The heat shield is integrated with the foreward propellant tank bulkhead, and the fins are extended from the engine fairings.

In the second approach (Fig. 2), an aerodynamically stable configuration is established by means of a suitable propellant tank arrangement. Stability is achieved if the nose radius of curvature is greater than the distance from the nose to the center of gravity The size of the heat shield influences the useful angle-of-attack range. A body of fineness ratio greater than unity will require the addition of either fins or flared afterbody to achieve a useful range of static stability. A body of low fineness ratio may be designed to be inherently stable over a useful angle-of-attack range. Orientation control is

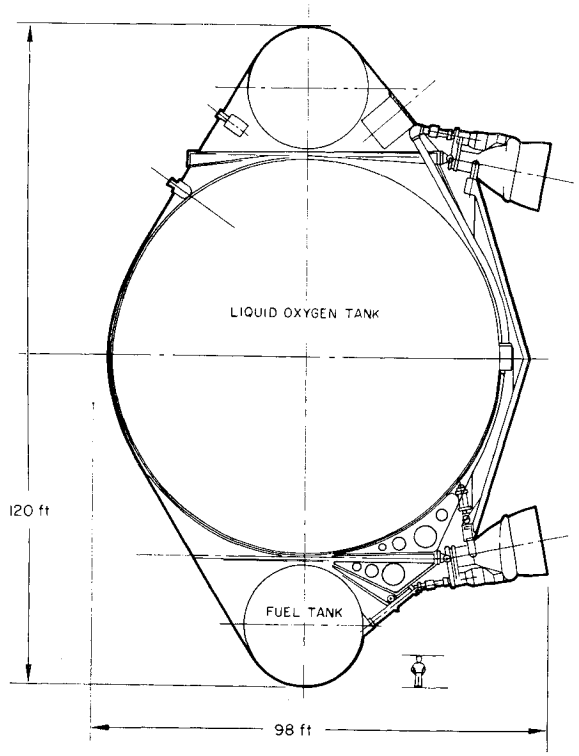

Fig. 2 Recoverable launch vehicle, configuration II.

required to assure proper initial atmosphere entry flight attitude, and stability augmentation is required. The principal advantage of this design approach is the low length-to-diameter ratio, which facilitates handling on the earth's surface.

Terminal deceleration devices that have been considered include parawings, rigid wings, rotors, balloons, parachutes, and retrorockets. The parawing[1] permits steering to a desired recovery area, except that first-stage boost trajectories preclude a return to the launch area and retrieval is probably not greatly assisted by steering to a point in midocean. Technical drawbacks include higher weight compared to parachutes and the necessity of deployment at relatively high dynamic pressure. Rigid wings would provide the same maneuverability as parawings, but would be the heaviest recovery device. Rotors can produce drag through autorotation, but NOVA stage recovery would require disks approximately 500 ft in diameter, and the concept collapses under practical design rationality. Large balloons could achieve buoyancy by heating captured ram air[2]; this technique would permit gentle touchdown in calm weather and could provide a solution to some of the handling problems.

In comparison to the preceding, the parachute is light and relatively well developed; 100-ft-diam cargo parachutes are in use, 200-ft-diam canopies have been fabricated experimentally, and diameters up to 300 ft would not exceed requirements for currently available parachute materials.[3] Figure 3 illustrates, in a general way, the relationship of parachute cluster dimensions to basic stage dimensions. Solid-propellant retrorockets also look promising, especially when used in conjunction with parachutes. High-thrust motors have been developed in a number of missile programs; for this application, accurately timed ignition (and hence precise height sensing equipment) is required.

Because of the large size of booster stages, an extension in the present state of the art is required for all recovery approaches considered. The booster vehicle itself presents size problems in the areas of design, manufacturing, and transportation, so that such problems should not be considered a serious deterrent to the applicability of recovery systems. The use of parachutes and solid-propellant rockets in combination

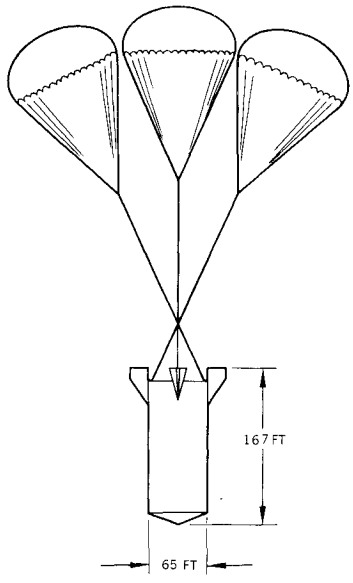

Fig. 3 Parachute recovery of NOVA launch vehicle stage.

offers the lightest system and requires the least extension of current technology. The decelerated recoverable launch vehicle stage is permitted to drop into the water. Alighting loads must be commensurate with other operational loads to achieve an efficient structural design. Shaping of the heat shield or forward bulkhead is important. The large empty volume of the propellant tanks eliminates the need for flotation devices.

Design Conditions

The vehicle must withstand atmosphere entry, terminal deceleration, and alighting on the open ocean and be acceptable for refurbishment. This constitutes one test for feasibility. The following analyses are based on recovery initiation velocities of 11,000 and 26,000 fps for the first and second stages, respectively.

Aerodynamic Loads

The maximum load factor experienced by an object decelerating in the atmosphere is a function of the initial conditions of velocity, altitude, and flight-path angle, and is essentially independent of ballistic coefficient. Nominal conditions of first-stage separation result in a peak load factor of 15 g's, which is a reasonable load level for the principal

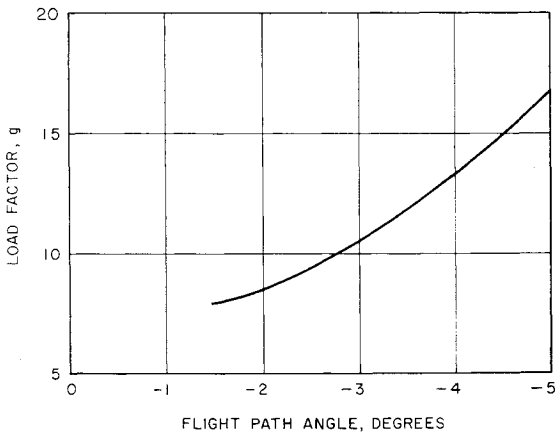

Fig. 4 Peak atmosphere entry load factor for orbital stage recovery.

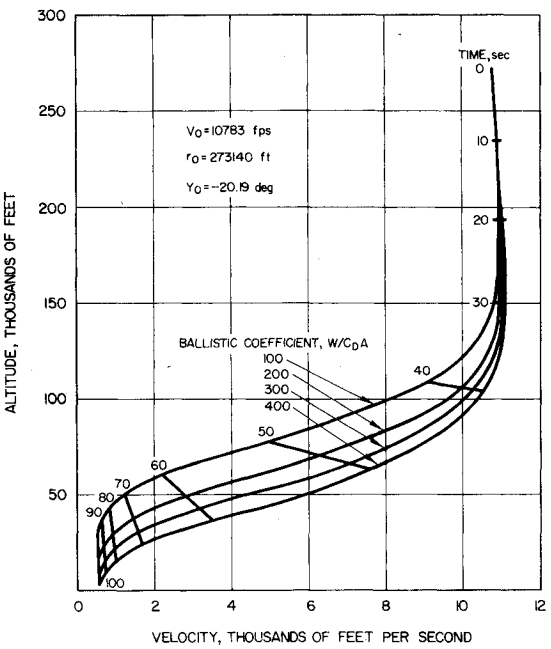

Fig. 5 Atmospheric entry profiles, suborbital recovery.

structural elements of the stage in view of the lightweight condition after first-stage burnout. Maximum load factor is not rapidly reduced by selecting a reduced separation velocity; the effect is nearly linear from 15 g at 11,000 fps to 11 g at 7500 fps. For the second stage, the effect of entry angle on peak longitudinal load factor is shown in Fig. 4. A maximum entry angle of $-4°$ is suggested to keep the load factor below 15 g, but the entry angle must be $\geq -2°$ to prevent skip-out.

Aerodynamic Heating

The calculation of aerodynamic heating during the atmosphere entry has been approached by means of the Kemp-Riddel equation for stagnation-point heating[4, 5]:

$$\dot{q}_c = 17{,}600\,(R_n)^{-1/2}\left(\frac{\rho_\infty}{\rho_0}\right)^{1/2}\left(\frac{V}{26{,}000}\right)^{3.25}\left[\frac{(h_s - h_w)}{(h_s - h_{300})}\right]$$

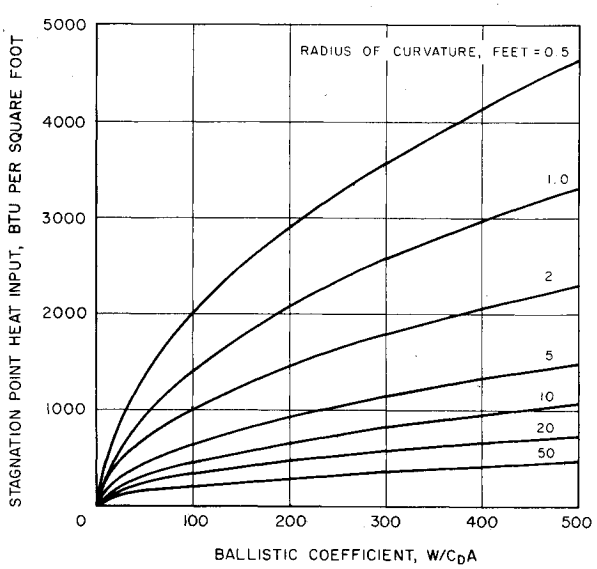

Fig. 6 Stagnation-point heat load to a low-temperature surface.

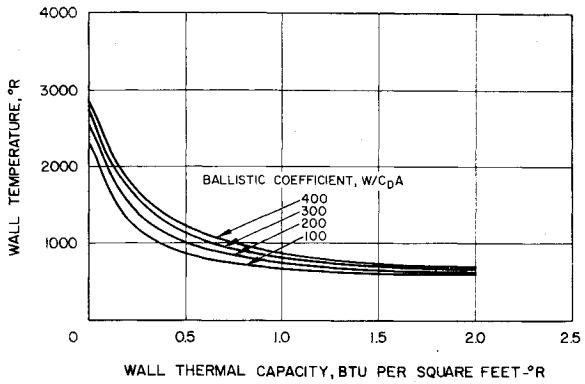

Fig. 7 Stagnation-point peak temperatures: radius of curvature = 50 ft.

Figure 5 shows typical first-stage trajectory data for objects with ballistic coefficients ranging from 100 to 400. Total heat input to a cool ablating surface is plotted in Fig. 6 as a function of the ballistic coefficient and nose radius. For nonablating surfaces, skin temperatures are dependent upon the thermal capacity and emissivity of the surface. Estimated peak temperatures at the stagnation-point vs wall thermal capacity for a nose radius of 50 ft are shown in Fig. 7. Insulation and ablative coatings may be used to provide thermal protection for thin exposed components. Large structures, which generally would be constructed with heavier skins, experience smaller heating rates, so that thermal protection may not be required for the major structural items.

Recovery of upper stages from earth orbit presents a more formidable design problem. Figure 8 shows typical deceleration profiles for an initial flight path angle of $-3°$ (measured from local horizontal plane) for bodies with ballistic coefficients of 50, 100, and 200 psf. The stagnation-point heat loads for R_n = 50 ft are shown in Fig. 9. Reduced heat loads at higher entry angles are due to shorter transit times. Ablative and/or insulative coatings are required for exposed structure.

Terminal Deceleration

Parachutes are employed to decelerate the recoverable body to a descent rate of the order of 100 fps, and then retrorockets decelerate it to an acceptable water entry velocity. For suborbital entry, subsonic speeds are attained at suitable parachute deployment altitudes, as indicated in Fig. 10. Subsonic speeds are achieved at even higher altitudes for

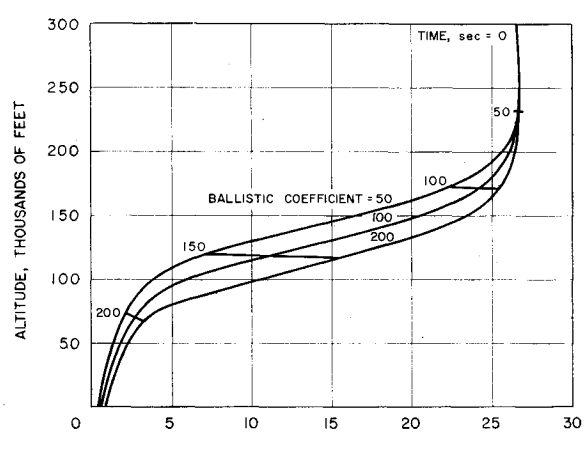

Fig. 8 Atmosphere entry profiles, oribital recovery.

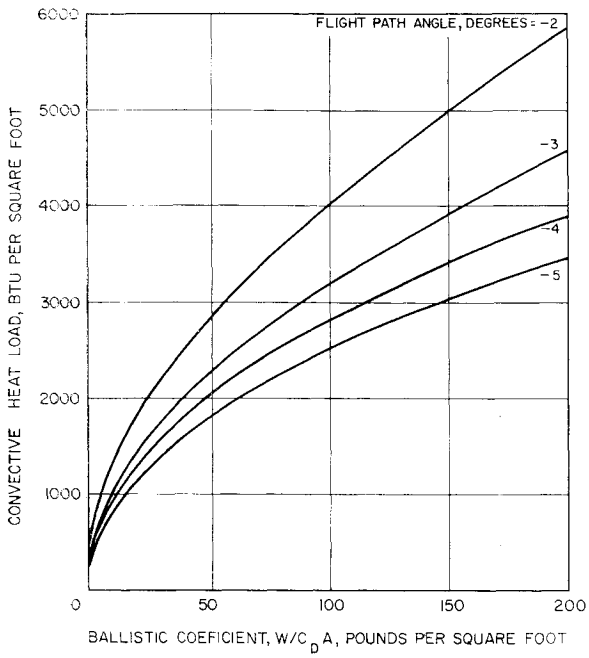

Fig. 9 Stagnation-point heat load, orbital recovery; $R_n = 50$ft.

orbital recovery operations because of the shallower entry flight-path angles utilized. Supersonic parachutes have been developed and tested in the range of Mach 1.0 to 2.0.[6] Drag balloons or cones are feasible to even higher speeds.

The load factor due to parachute-opening shock determines the strength (hence weight) required. A typical configuration with $W/C_DA = 350$ psf will have a velocity of 1050 fps at 20,000-ft alt, giving a dynamic pressure of 770 psf but at 100 fps at sea level, the dynamic pressure is only 11.9; psf (Fig. 10). Thus four and perhaps five stages of deceleration are desirable. For this case, four stages would be recommended. These stages would typically consist of a reefed fist-ribbon type of drogue chute, disreefed drogue chutes, reefed main chutes, and disreefed main chutes.

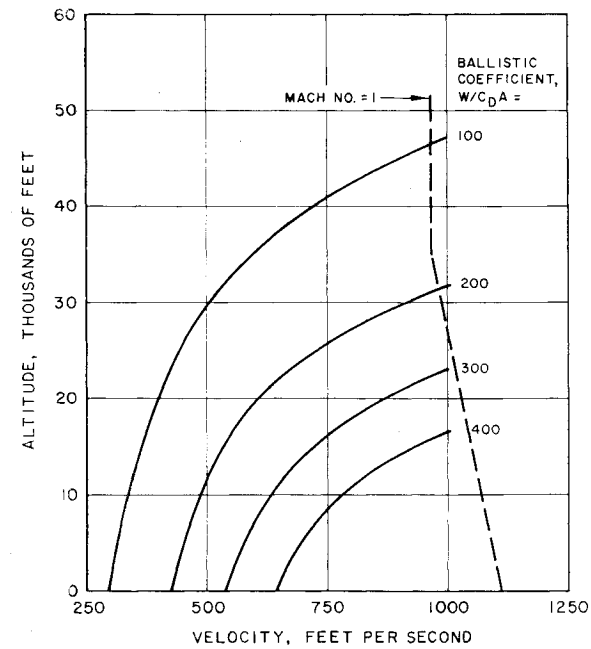

Fig. 10 Terminal altitude-velocity profile, suborbital recovery.

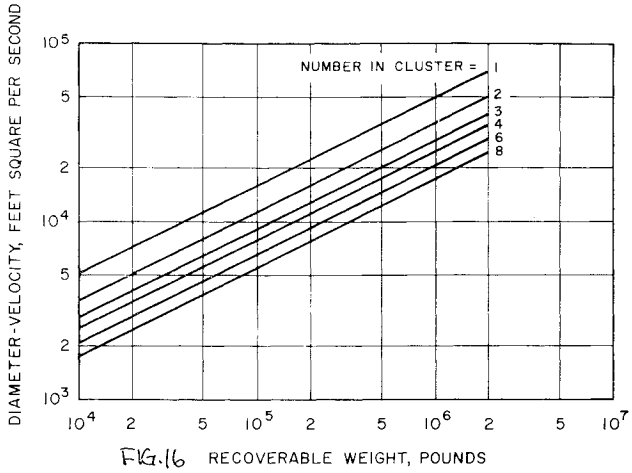

Fig. 11 Parachute cluster selection chart, fist-ribbon-type.

The massiveness of recoverable booster stages presents the single greatest departure from current parachute recovery practice. Parachute clusters offer advantages in smaller size and improved dynamic stability. Clusters of three to seven of the flat circular type have been observed to exhibit oscillations of less than 5°.[6, 7] Cluster data are presented on Figs. 11 and 12 for fist-ribbon and flat-circular parachute clusters, respectively. A 10^6-lb stage can be decelerated to a velocity of 250 fps by four 100-ft-diam fist-ribbon drogue parachutes. A cluster of four 200-ft-diam flat-circular parachutes is required to achieve a terminal descent rate of 100 fps. A single parachute to achieve the same terminal descent rate would have to be 400 ft in diameter. Weights of individual parachutes are shown in Fig. 13 for the deployment conditions noted. These weights assume the use of a large number of medium-strength suspension lines; e.g., a 100-ft-diam fist would require 180–10,000-lb-test suspension lines. Main parachutes would use an even larger number of lower-strength suspension lines to minimize weight. Figure 14 shows estimated parachute system weight as a fraction of recovered weight.

A brief analysis of the dynamics of the vehicle during retrorocket operation in the final phase of descent is as follows. The equation of motion is

$$W\dot{V}/g = W - F - C_D \rho V^2/2g$$

It is assumed that terminal descent velocity has been achieved

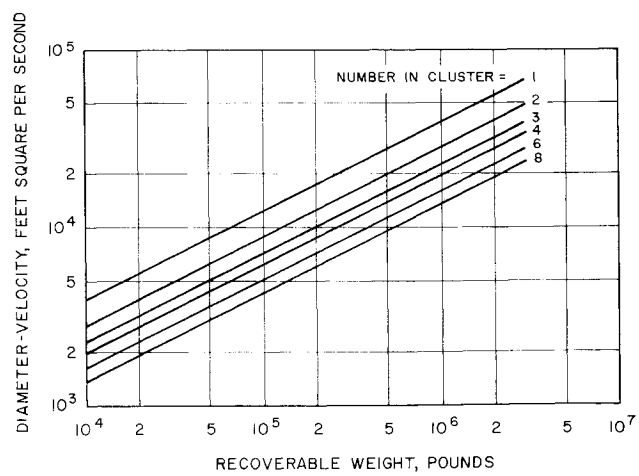

Fig. 12 Parachute cluster selection chart, flat-circular-type.

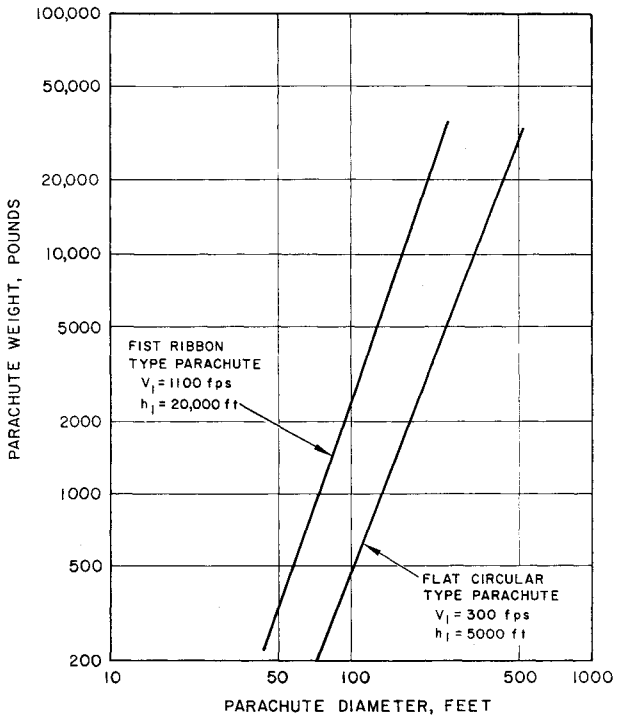

Fig. 13 Parachute weight characteristics.

prior to the ignition of the rocket decelerators. The rate of descent as a function of time during firing is given by

$$\tan^{-1}N^{-1/2} - \tan^{-1}(V/V_0N^{1/2}) = gt/V_0N^{1/2}$$

where $N = (F/W) - 1$. The time required to decelerate to a hovering condition with zero rate of descent is

$$t = (V_0/gN^{1/2}) \tan^{-1}N^{-1/2}$$

Thus t/V_0 is a function only of N, or the thrust-weight ratio.

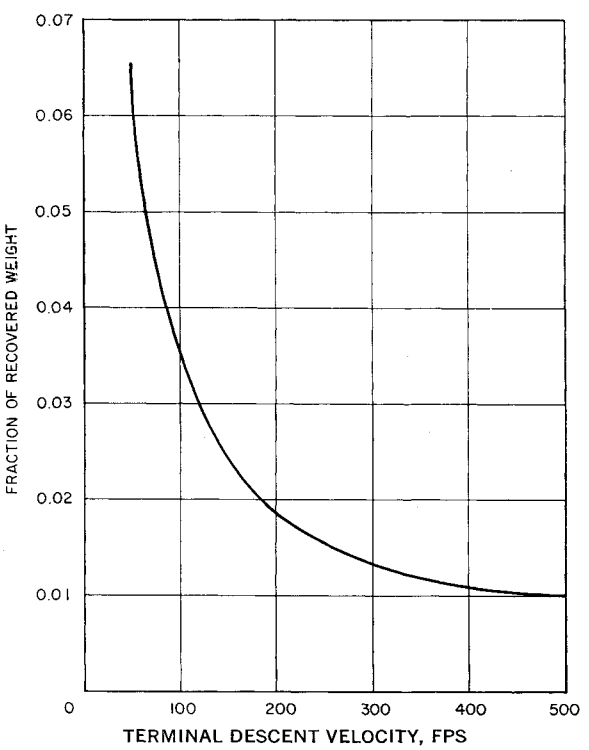

Fig. 14 Parachute deceleration system, weight fraction.

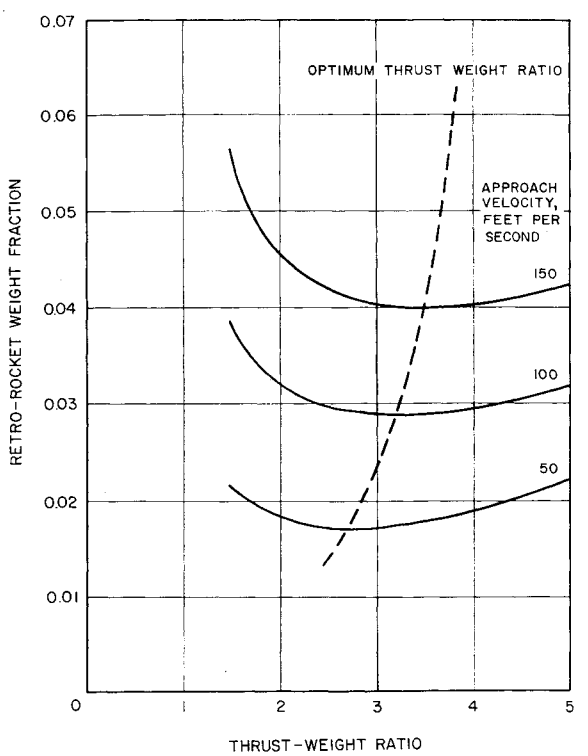

Fig. 15 Retardation rocket-vehicle weight ratio.

Rocket motor inert weights may be divided into a fraction that is dependent on thrust and a fraction that is dependent on propellant loading. Thus

$$W_r = AF + BW_p + W_p$$

Dividing by total vehicle weight W and setting $W_p = Ft/I_s$

$$W_r/W = (F/W)[A + (1 + B)t/I_s]$$

Curves of typical retrorocket weight fraction for deceleration to a hover condition are shown in Fig. 15. Results from Figs. 14 and 15 lead to an optimum recovery system when the parachute subsystem is designed for a terminal descent rate of approximately 120 fps (Fig. 16).

Variances in parachute drag loss with one parachute missing, altimetry, rocket ignition time, impulse, and the effects of ocean surface waves lead to the expected maximum deviations shown in Table 1. It is extremely improbable that maximum rate of descent should occur simultaneously with maximum hover height. An elliptical distribution is proposed as a design criterion as illustrated in Fig. 17. This curve is tangent to the altitude-velocity plot for a free fall from a height of 14 ft. The resultant alighting velocity is 30 fps. It is suggested that this be used for a design condition for the determination of water entry loads. A small improvement may be achieved by designing the retrorocket deceleration system to bring the vehicle to rest a few feet above the surface of the water.

Water Alighting Loads

The parachute-retrorocket retardation system has been shown to require a design water entry velocity of 30 fps. If a parachute retardation system is employed without the aid of retrorockets, it generally will be necessary to design for water entry velocities of 70 fps or greater for large recovery items. Alighting load investigations must also consider the state of the water surface. Waves up to 12 ft and surface winds up to 40 knots should be considered. This will assure a high probability that the actual sea state will be less severe.[8]

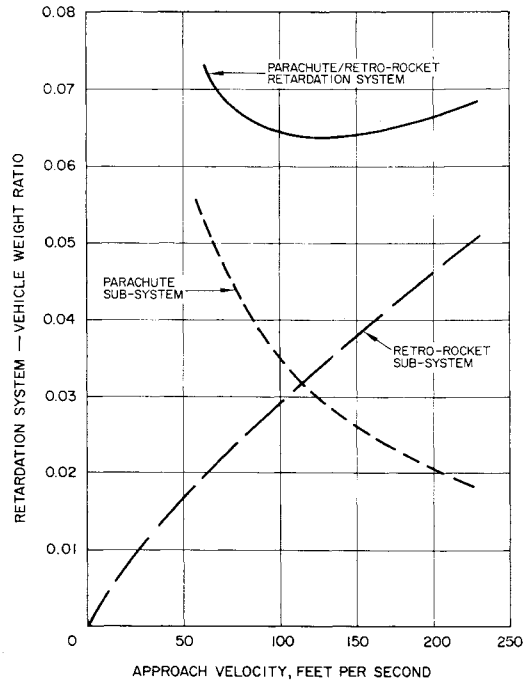

Fig. 16 Parachute-retrorocket retardation system, weight fraction.

The final design consideration is that the blast from the retrorockets will tend to displace the water immediately below the vehicle. This effect is considered desirable because the alighting loads will be shifted away from the center and toward the sides of the vehicle.

Alighting loads for smooth water are determined by a momentum exchange principle. The momentum of the descending vehicle is equated to the total momentum of the vehicle and displaced water, which is considered to be equal to three-fourths of the water contained in a hemisphere of diameter equal to the wetted diameter of the vehicle[9]:

$$WV_0 = [W + (\pi/2)\rho y^3]V$$

The lateral offset y is related to the depth of penetration x by the equation of the generatrix of the surface entering the water. For a conical surface, $y = K_1x$; hence

$$V = V_0/(1 + K_2x^3)$$

where $K_2 \equiv \pi K_1^{3/2}(\rho/W)$, which is in feet^{-3}, and $(1 + K_2x^3)$ is dimensionless. The deceleration and average pressure loading are

$$a = 3K_2V_0^2x^2/(1 + K_2x^3)^3$$

$$p = 3K_1\rho V_0^2/2g(1 + K_2x^3)^3$$

Typical results are plotted in Fig. 18 for a cone with dead rise angle of 10°. Peak acceleration and the velocity and depth at which it occurs are

$$a_{max} = -0.72\ K_1V_0^2(\rho/W)^{1/3}$$

$$V_{a_{max}} = 0.78\ V_0$$

$$x_{a_{max}} = 0.566\ (W/\rho)^{1/3}/K_1$$

Peak load factor vs V_0 is plotted in Fig. 19 for several cones. The curves nominally apply to 10^6-lb vehicles but may be adjusted by the ratio $(10^6/W)^{1/3}$. Since the depth of penetration for maximum acceleration is independent of the approach velocity, the maximum load occurs over the same area for normal approaches.

For a paraboloid of revolution, the surface generatrix is $y = K_3x^{1/2}$, which also applies for a spherical surface with $K_3 = (2R_n)^{1/2}$, and

$$V = V_0/(1 + K_4x^{3/2})$$

$$a = 3K_4\ V_0x^{1/2}/2(1 + K_4x^{3/2})^3$$

$$p = 3\rho\ K_3\ V_0x^{-1/2}/4g(1 + K_4x^{3/2})^3$$

where $K_4 \equiv \pi K_3^{3/2}(\rho/W)$. Peak acceleration and the velocity and depth at which it occurs are

$$a_{max} = -0.715\ K_3^2V_0^2\ (\rho/W)^{2/3}$$

$$V_{a_{max}} = 0.889\ V_0$$

$$x_{a_{max}} = 0.425\ (W/\rho)^{2/3}/K_3$$

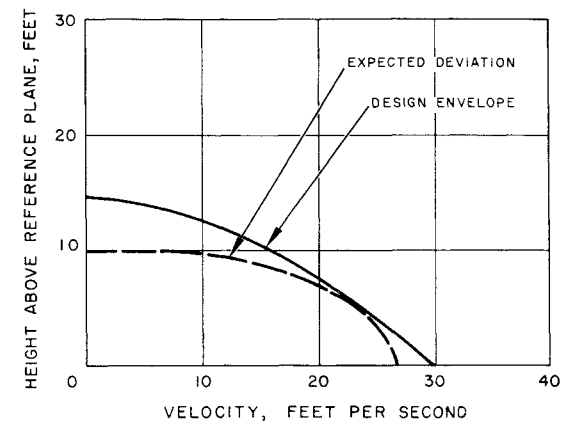

Fig. 17 Water impact structural design criteria.

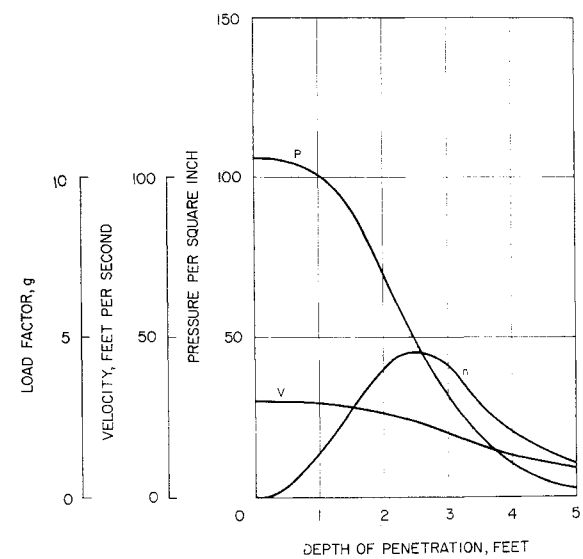

Fig. 18 Water impact transients for cone with 10° deadrise angle.

Table 1 Three-sigma deviations for parachute-retrorocket retardation system

Source of deviation	Altitude, ft	Velocity, fps
Air temperature, ±50°F	0	±5
Parachute missing, 1 of 8	0	+7
Altimetry, ±2%	±2	0
Rocket ignition, ±0.05 sec	±6	0
Rocket thrust, ±5%	+6, −7	+25, −2
Rocket impulse, ±2.5%	±0.05	±3
Surface waves, 12 ft	±6	±3
Cumulative deviation, root-sum-square	±10, −11	+27, −7

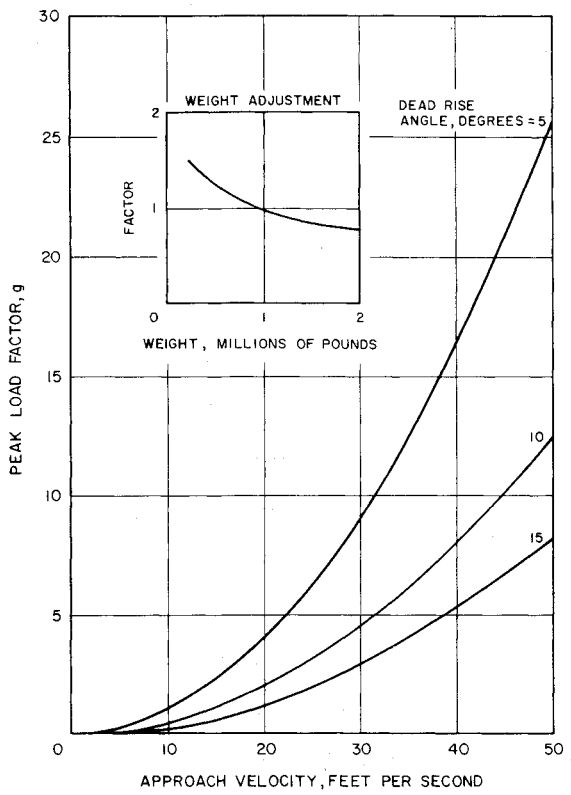

Fig. 19 Alighting loads on cones: $W = 10^6$ lb.

Peak alighting loads are shown in Fig. 20.

It is concluded that the water alighting loads are approximately 10 g's peak. This is compatible with other design conditions, so that it is not expected that severe weight penalties would be incurred to design for water alighting loads.

Economic Considerations of Launch Vehicle Recovery

The expected number of re-uses for a launch vehicle stage may be estimated by considering the reliability of the complete cycle from launch through separation, atmosphere entry, terminal deceleration, water entry, retrieval, and refurbishment, transport, assembly, and erection for the next launch. The expected number of launches per vehicle is the sum of the launch probabilities over the permissible number of attempts.

The reliability of the first-stage operation from launch to separation should be at least 0.9. Because the vehicle is too heavy during the launch phase for the recovery systems to operate satisfactorily, it is assumed that an aborted launch leads to loss of the first stage. The reliability of recovery operations should also be at least 0.9, so that the launch-recovery cycle should have a reliability greater than 0.8, which would improve with time. However, a considerable time will be required for refurbishment of such large vehicles, and in any program the process of improving reliability must be terminated somewhat arbitrarily. For example, vehicle production for a ten-year program could be scheduled for the first three years, followed by refurbishing operations for the remaining seven years, during which time it might be expected that a given vehicle might experience one launch attempt per year. If this is the case, launch-recovery cycle reliability greater than 0.88 would result in an average of 6 launches/vehicle. Thus it does not appear to be imperative to develop extremely high recovery cycle reliability to achieve useful results on a program. If large inventories of launch vehicles are available for specific mission objectives, then the expected number of launch attempts per vehicle will either diminish or the program may be expanded to take advantage of the remaining launch vehicles.

Recoverable first- and second-stage weights are based on an increase of the vehicle empty weight fraction of 17 and 25%, respectively, as compared to expendable stages. Table 2 presents estimated vehicle weights and program costs for an expendable vehicle, a vehicle with recoverable first stage, and a vehicle with both stages recoverable. Each vehicle would place a 10^6-lb payload into a low-altitude earth orbit, using oxygen-kerosene in the first stage and oxygen-hydrogen in the second. The launch program is assumed to require 100 launch attempts.[10] For recoverable stages, it is assumed that 25 units are required to provide flexibility in mission assignment.

Manufacturing costs are based on an 85% learning curve with production costs of \$40/lb on the 100th production unit.[11] Propellant costs are estimated at \$0.03/lb for oxygen-kerosene and \$0.13/lb for oxygen-hydrogen. Recovery operations and retrieval costs are comparable with transportation costs, which are assumed to be relatively small. Refurbishment costs are based on a vehicle designed for recovery operations. Therefore refurbishment of the structure and propulsion systems should not be extensive for the limited number of expected launches. Recovery systems require major refurbishment but account for only 6.5% of the total manufactured cost. Flight acceptance firings and systems checkout represent operation costs that do not appreciably vary for an expendable program or a recoverable program. The retrieval and refurbishment cost per recovery cycle is therefore estimated to be 10% of the manufacturing costs. Development costs are assumed to be equal to \$2000/lb based on stage empty weight.

Table 2 indicates that a launch vehicle with a recoverable first stage will show a direct operating cost 33% smaller than that of a fully expendable launch vehicle. Recovering both stages would reduce direct operating cost (DOC) by 36%. The DOC savings are somewhat offset by increases in developmental costs, so that the net savings are 20% for

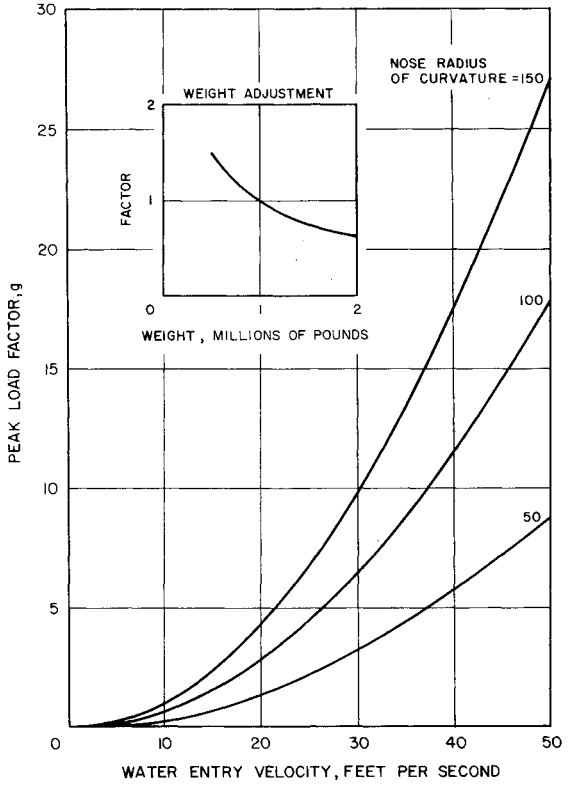

Fig. 20 Alighting loads on spheres and paraboloids of revolution $W = 10^6$ lb.

Table 2 Estimated vehicle weights and program costs for 100-launch program with 10^6-lb payload vehicle

Item	Both stages expend.	First stage recov.	Both stages recov.
Weights, 10^6 lb			
First stage	22.2	23.9	26.2
Dry	1.6	2.0	2.2
Propellant	20.6	21.9	24.0
Second stage	3.55	3.55	4.00
Dry	0.37	0.37	0.50
Propellant	3.18	3.18	3.50
Total (incl. W_{pay})	26.8	28.4	31.2
Costs, $\$10^9$			
First stage	8.42	4.65	5.12
Manufacturing	8.35	3.52	3.88
Recov. and refurb.	...	1.06	1.16
Propellant	0.07	0.07	0.08
Second stage	1.98	1.98	1.19
Manufacturing	1.93	1.93	0.88
Recov. and refurb.	...	...	0.26
Propellant	0.05	0.05	0.05
Operations	1.00	1.00	1.00
Sub total, DOC	11.40	7.63	7.37
Developmental	3.94	4.74	5.40
Total cost	15.34	12.37	12.71

first-stage recovery but only 17% for recovery of both stages. However, considerations of reliability improvement and program timing requirements (manpower) could be used to justify second-stage recovery. Programs that involve larger numbers of launches with smaller launch vehicles are more adaptable to recovery and might show greater percentage savings than is indicated by the preceding analysis.

Concluding Remarks

Recovery of large-size booster stages has been shown to be feasible from the standpoint of flight and water alighting loads. Retrieval and refurbishing operations have not been examined, but it is expected that approaches can be implemented which will not result in excessive structural loads or insurmountable handling problems. It is noted that the second design approach would float on the water with the rocket engines protected from saltwater immersion. This could be a problem for the conventional configuration design approach.

The question of recovery clearly is related to the size of space operations to be undertaken in the future. Analysis of past and current trends in space operations indicates an exponential growth.[10] The smallest program that would marginally benefit from recovery is estimated to involve 30 launches with 11 recoverable vehicles.

References

[1] Hatch, H. G., Jr. and McGowan, W. A., "An analytica investigation of the loads, temperatures, and ranges obtained during the recovery of rocket boosters by means of a parawing," NASA TN D-1003 (February 1962).

[2] Oberg, A. J., Sopezak, S. S., and Sutton, M. A., "Paravulcoon recovery and landing system," Aeronautical Systems Div. Retardation and Recovery Symposium Proceedings (November 1962).

[3] "Performance and design criteria for deployable aerodynamic decelerators," Aeronautical Systems Div. TR 61-579 (December 1963).

[4] Kemp, N. H. and Ridell, F. R., "Heat transfer to satellite vehicles re-entering the atmosphere," Jet Propulsion **27**, 132–137 (1957).

[5] Detra, R. W., Kemp, N. H., and Ridell, F. R., "Addendum to 'Heat transfer to satellite vehicles re-entering the atmosphere,' " Jet Propulsion **27**, 1256–1257 (1957).

[6] Pedersen, P. E., "Study of parachute performance at low supersonic deployment speeds; effects of changing scale and clustering," Aeronautical Systems Div. TR 61-186 (July 1961).

[7] "Wind tunnel study of parachute clustering," Flight Accessories Lab., Aeronautical Systems Div. TDR 63-159 (April 1963).

[8] "North Atlantic Ocean," *U. S. Navy Marine Climatic Atlas of the World* (U.S. Weather Bureau, Direction of Chief of Navy, Washington, D. C., 1955), Vol. I.

[9] McGee, J., Hathaway, M., and Vaughn, V., "Water-landing characteristics of a re-entry capsule," NASA Memo. (May 23, 1959).

[10] Koelle, H. H., "Trends in earth-to-orbit transportation systems," Astronaut. Aerospace Eng. **1**, 25–30 (October 1963).

[11] Koelle, H. H., *Handbook of Astronautical Engineering* (McGraw-Hill Book Co., Inc., New York, 1961).